INL/EXT-08-14039

Evaluation of Heterogeneous Options: Effects of MgO Versus UO_2 Matrix Selection for Minor Actinide Targets in a Sodium Fast Reactor

Michael Pope
Samuel Bays
Rodolfo Ferrer

March 2008

The INL is a U.S. Department of Energy National Laboratory
operated by Battelle Energy Alliance

INL/EXT-08-14039

Evaluation of Heterogeneous Options: Effects of MgO Versus UO_2 Matrix Selection for Minor Actinide Targets in a Sodium Fast Reactor

Michael Pope
Samuel Bays
Rodolfo Ferrer

March 2008

Idaho National Laboratory
Idaho Falls, Idaho 83415

http://www.inl.gov

Prepared for the
U.S. Department of Energy
Office of Nuclear Energy
Under DOE Idaho Operations Office
Contract DE-AC07-05ID14517

Evaluation of Heterogeneous Options: Effects of MgO versus UO_2 Matrix Selection for Minor Actinide Targets in a Sodium Fast Reactor

INL/EXT-08-14039

March 2008

Approved by

Michael Pope, Principal Author	Date
Mehdi Asgari, Department Manager	Date
Kathryn McCarthy, Systems Analysis Campaign Director	Date

Executive Summary

The primary focus of this work is a comparison between MgO and UO_2 as matrix material options for burning minor actinides (MA) in transmutation targets within a sodium cooled fast reactor. The heterogeneous sodium fast reactor considered in this analysis was adapted from the homogeneous Advanced Burner Reactor.[2] In a previous work by Idaho National Laboratory, MgO and UO_2 target matrix options were compared based on identical target geometry.[3] Thus, the TRU conversion ratio (CR) was allowed to change due to excess TRU breeding in the UO_2 matrix. In this work, the fuel volume fraction was changed in order to match the CR between the UO_2 and MgO cases at approximately 0.75. This was done in order to provide a comparison of the two matrix materials based on similar net TRU destruction rates. The number of target assemblies was kept the same in each heterogeneous case (48) and approximately the same cycle length was used since it was limited by the fluence in the outer driver zone. The cycle length was set by limiting each assembly in the core to 200 dpa during its life. Also, the mass ratio of MAs (Am+Cm+Cf+Bk) to Np+Pu in the external supply of TRU was held constant and equal to that found in LWR SNF. For the purpose of this study, neptunium is excluded from the definition of "minor actinide".

The UO_2 matrix-based targets required a 30% higher MA loading in order to achieve the same *net* MA destruction rate as the targets with an inert MgO matrix. The larger MA loading for the UO_2 case is due to the fact that the UO_2 case has a smaller transmutation efficiency than the MgO case. The MA destruction efficiency (EMA) of the targets is defined as the absolute value of the MA mass in a target assembly at discharge minus the amount charged in a fresh assembly, divided by the amount in the fresh assembly. The transmutation efficiency is 33% and 43%, for the UO_2 and MgO case respectively. The reduced transmutation efficiency of UO_2 is caused by the breeding of TRU from U-238 during the target's 10 cycle irradiation. During the irradiation time, the successive neutron captures from this bred TRU, eventually produce and accumulate MAs within the target. Due to the introduction of this internal source of MAs in the fuel cycle of the UO_2 matrix, the MA charge rate must be increased in order to maintain the same net MA destruction rate as in the MgO case. This is achieved by increasing the MA concentration in the targets (target enrichment).

Assuming that the two matrix materials release the same fraction of fission gasses produced, the higher MA actinide inventory present in the targets having UO_2 matrix leads to higher fission gas pressures in the target pins, since they will have more fissions occurring during their core residence time. In this analysis, the calculated gas pressures in the UO_2 matrix targets were higher still due to the lower fuel volume fraction in these targets. However, even if compared on a basis of equal space available for fission gas release, the targets having UO_2 matrix would have higher pressures at discharge due to their larger number of fissions during the target lifetime. In addition, the larger MA inventory in the UO_2 targets can lead to a greater helium release due to alpha decay of minor actinides, particularly curium and americium.

DISCLAIMER

ACKNOWLEDGEMENTS

The authors would like to thank Steve Piet (INL) for his technical contributions.

CONTENTS

FIGURES

TABLES

GLOSSARY, ACRONYMS, AND ABBREVIATIONS

ANL	Argonne National Laboratory
BOEC	Beginning of Equilibrium Cycle
BOL	Beginning of Fuel Life
CR	Conversion ratio
EOEC	End of Equilibrium Cycle
EOL	End of Fuel Life
LWR	Light Water Reactor
MA	Minor Actinides (excluding neptunium, which is included with TRU for this analysis)
MC^2-2	Code System for Calculating Fast Neutron Spectra and Multigroup Cross-Sections
MOX	Mixed Oxide
ORNL	Oak Ridge National Laboratory
RGU	Reactor Grade Uranium
REBUS-3	Reactor Burnup Code System for Analysis of Fast Reactor Fuel Cycles
SFR	Sodium Fast Reactor
SNF	Spent Nuclear Fuel
S-PRISM	Super - Power Reactor Innovative Small Module
TRU	Transuranics
UOX	Uranium Oxide
UREX	Uranium Extraction Process

1. Introduction

Recent consideration of heterogeneous transuranic (TRU) burning sodium fast reactor (SFR) core designs has prompted the investigation of burning minor actinides (MA) in dedicated target assemblies. Two options under consideration for a carrying matrix in the MA targets are UO_2, with the uranium having the isotopic composition equivalent to that of natural or recovered uranium, and inert matrix. In this work we consider MgO as the inert matrix material and recovered uranium for the isotopic composition of the UO_2.

The analysis considered a TRU burning core wherein the MAs from light water reactor (LWR) spent nuclear fuel (SNF) and the MAs generated by the SFR driver fuel are partitioned in the fuel cycle and burned in 48 heterogeneous targets located in the core periphery. The residence time of any driver or target assembly is limited by a maximum cladding damage criterion of 200 displacements per atom (dpa) or effectively a fast neutron fluence of approximately 4×10^{23} cm^{-2} (>100 keV) [1]. After irradiation, the targets are reprocessed and the plutonium and neptunium (Np+Pu) created during the irradiation is loaded back into the driver fuel. The MAs discharged from the target irradiation are recycled and reconstituted into the next reactor pass of targets. The Np+Pu remaining in the discharged driver elements is returned to the driver elements and the MAs in the discharged drivers are sent to the target assemblies. Hence, the Np+Pu and the MAs in this scenario are multi-recycled as opposed to a once-through-then-out scenario.

The heterogeneous sodium fast reactor considered in this analysis was adapted from the homogeneous Advanced Burner Reactor [2]. In a previous work by Idaho National Laboratory, MgO and UO_2 target matrix options were compared based on identical target geometry.[3] Thus, the TRU conversion ratio (CR) was allowed to change between the two cases due to excess breeding in the UO_2 matrix option. In this work, the fuel volume fraction was changed in order to match the CR between the UO_2 and MgO cases. Also, the mass ratio of MAs to Np+Pu in the external supply of TRU was held constant and equal to that found in LWR SNF. The same number of target assemblies was used in each heterogeneous case (48) and approximately the same cycle length was used, since it was limited by the fluence in the outer driver zone.

2. Methodology

2.1 Reactor Physics and Fuel Cycle Simulation

The Argonne National Laboratory fast reactor codes MC^2-2, DIF3D and REBUS were used for the reactor physics and fuel cycle calculations [4,5,6]. The MC^2-2 code was used to generate a 33 group cross section set for each driver fuel enrichment zone, the targets, reflectors and shields. Starting with an ultra-fine group ENDF-V/B cross section library, MC^2-2 creates a collapsed cross section set by performing a zero dimensional infinite dilution critical buckling search using the extended P1 method [4]. Using this collapsed cross section set, the DIF3D diffusion code was used to solve the multi-group steady state neutron diffusion equation using a hexagonal-z nodal coordinate system [5]. In the nodal discretization, each hexagonal node in the lateral direction represents an assembly. REBUS uses DIF3D to perform a criticality search for the uncontrolled excess reactivity at each time step in its fuel depletion algorithm [6]. In this search, the fresh fuel transuranic enrichment is adjusted until enough beginning-of-equilibrium-cycle (BOEC) excess reactivity is present to keep the core critical until the end-of-equilibrium-cycle (EOEC). For each enrichment adjustment, the fluxes from DIF3D are used to carry out the isotopic buildup/depletion process over the time of the irradiation cycle. REBUS also performs the in-core fuel management and out-of-core cooling, reprocessing and re-fabricating for each reactor cycle. These operations are carried out until the BOEC excess reactivity is found for the prescribed cycle length.

The ratio of MAs (Am+Cm+Bk+Cf) to Np+Pu in the external supply of transuranics was held constant and equal to the actual ratio found in LWR SNF. Because this ratio was always respected in conjunction with a constant thermal power rating and an invariant CR, the external makeup feed rate of each isotope was also relatively invariant throughout this study. This made possible a comparison between the two matrix materials based on an equal rate of net destruction of external MA and Np+Pu.

2.2 Helium Generation and Pin Pressure Calculations

Since the REBUS calculation does not report total number of helium atoms produced in its output, a post processing code was developed to recreate the fuel buildup/depletion algorithm performed by REBUS. This was done in order to reproduce the detailed alpha decay history of the fuel as a function of irradiation time. The depletion algorithm uses an exponential matrix method to calculate the number density of each actinide isotope as a function of discrete time steps: $N_i(t)$ or N_i^t. Since the depletion history of the fuel is constructed in much finer time steps t than reported in the REBUS output, these number densities can then be converted into alpha decay activity. For the helium calculation, pure exponential decay is assumed within each time step (Δt). Once the N_i vector is found for all T time steps, a vector for decay activity is defined by multiplying the number of isotope atoms (i) in each row by its alpha decay constant (λ_α). Assuming that the change in N_i over Δt is negligible, the total number of decays in Δt, can be found by simply multiplying the activity by Δt.

$$N_{He}^{(t+\Delta t)-t} = \frac{dN_i^t}{dt} \times \Delta t = \lambda_\alpha^i \times N_i^t \times \Delta t \qquad (1)$$

However, in an effort to reduce the necessary time steps to give acceptable accuracy, a slightly more rigorous integration technique within the time step is applied. First, the activity within the time step is defined as:

$$A_i^t = \frac{dN_i^t}{dt} = -\lambda_\alpha^i \left(N_i^t e^{-\lambda_\alpha^i \times (\Delta t)} \right) \tag{2}$$

Where: A_i is the activity or rate of decay of isotope *i*. The helium production in the time step is found by integrating equation 2 over *t'*.

$$N_{He}^{(t+\Delta t)-t} = -\lambda_\alpha^i N_i^t \int_t^{t+\Delta t} e^{-\lambda_\alpha^i \times (t')} dt' = N_i^t \left(1 - e^{-\lambda_\alpha^i \times (\Delta t)} \right) \tag{3}$$

The total helium generation over the irradiation time is found by taking the sum of the solution to equation 3 over all time steps. A similar technique is used to calculate the atoms of krypton and xenon fission gas atoms produced by fission. Instead of λ_α, the fission reaction rate, in conjunction with the fission yield for krypton and xenon, is used instead: $B_{Kr}\sigma\phi$ and $B_{Xe}\sigma\phi$. The total fission gas yield for U-Pu fuel in a SFR is about 27% [7]. This percentage accounts for all intermediate short lived decays, following fission, that ultimately lead to formation of a stable Kr or Xe atom.

3. Assumptions and Models

3.1 Reference Core Design

The reference core design used in this work is derived from the oxide fueled Advanced Burner Reactor (ABR) with a CR of 0.75 originally proposed by Hoffman et al in ANL-AFCI-177 [**Error! Reference source not found.**]. This core is modified from the homogeneous geometry ABR to accommodate a heterogeneous recycling scheme utilizing 48 MA targets located in lieu of the first row of reflector assemblies. Figure 1 shows the layout of the 1/3 symmetric core used in this analysis.

The number of each type of assembly (in the full core) is given next to the labels in the key. The driver fuel is divided into three zones with varying enrichment. These enrichment zones (inner, middle and outer) are used to provide flattening of the radial power profile. Their enrichments vary but they do so in such a way that the different values are proportional to the factors 1.0, 1.25 and 1.5, respectively. The target enrichment is varied separately external to the REBUS code in order to preserve the MA to Np+Pu external feed ratio. The core also uses 16 primary control assemblies and three ultimate shutdown assemblies.

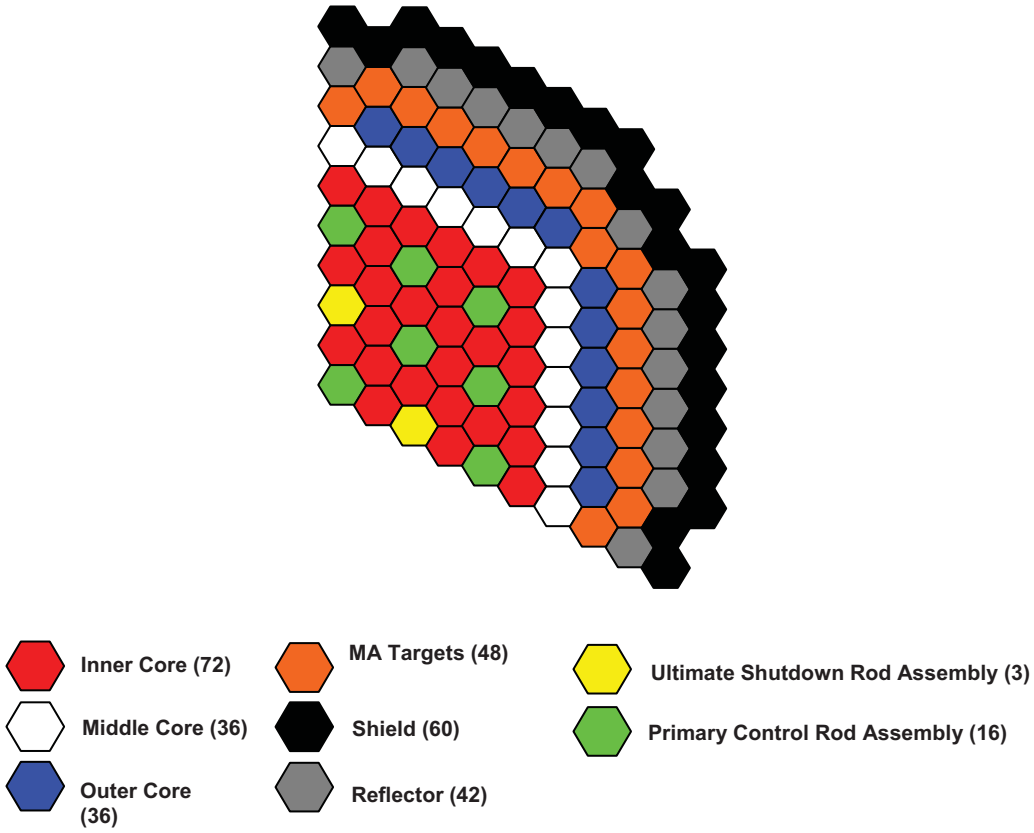

Figure 1. Heterogeneous core design arrangement having 1/3 core symmetry

Table 1 gives some core parameters of interest for the design used in this analysis. In the table, the word "Varied" is given to mean that these values were changed in the analysis in order to adjust the fuel volume fraction and thus the TRU CR.

The assemblies in the inner, middle and outer fuel regions are left in the core for 6, 6 and 7 cycles, respectively. The MA target assemblies, because they are in such a low-flux region of the reactor are left in the core for 10 cycles.

Table 1. Pin and assembly design.

Fuel Type	Oxide
Assembly pitch, cm	16.142
Inter-assembly gap, cm	0.432
Duct outside flat-to-flat, cm	15.710
Duct material	HT-9
Duct thickness, cm	0.394
Pins per assembly	271
Spacer type	Wire wrap
Bond material in gap	He
Plenum height, cm	170.82
Core height, cm	137.16
Axial reflector height, cm	114.30
Overall pin length, cm	422.28
Fuel smeared/fabrication density, % TD	85/89.4
Pin outer diameter, cm	Varied
Cladding thickness, cm	0.0635
Spacer wire wrap diameter, cm	Varied

3.2 Recycling Scheme

The separation and recycling strategy investigated in this work assumes the ability to partition uranium, Np+Pu, and MAs (Am+Cm+Bk+Cf) into three separate waste streams. The separation strategy is outlined in Figure 2. The general philosophy of maintaining the MA inventory in transmutation targets is indicated by the hot-cell and glove-box images at the center of the figure. In each recycle, the Np+Pu produced by the targets is separated from the MAs and recycled into the next batch of driver fuel. The driver external makeup feed is comprised of LWR SNF Np+Pu and recovered uranium (uranium recovered from SNF). Also in each recycle, the Am+Cm+Bk+Cf produced by the driver fuel is separated from the Np+Pu and recycled into the next batch of targets. The transmutation target external makeup feed of MAs has the same isotopic vector as the Am+Cm+Bk+Cf corresponding to LWR SNF.

The targets are irradiated on a multi-batch basis. As opposed to some "once-through-then-out" strategies, a "batch" fraction (i.e.: 48 targets/10 cycles = 4.8 targets per cycle) of the targets are removed, recycled and replaced with fresh targets every cycle. This ensures that only the losses in the transuranic reprocessing are sent to a geologic disposal. Since the ratio of Np+Pu to Am+Cm+Bk+Cf in the external TRU feed rate is always respected, as is the TRU CR, the amount of MA throughput in the core is approximately conserved for the two heterogeneous designs (i.e.: UO_2 vs. MgO target matrix options) of primary interest in this work.

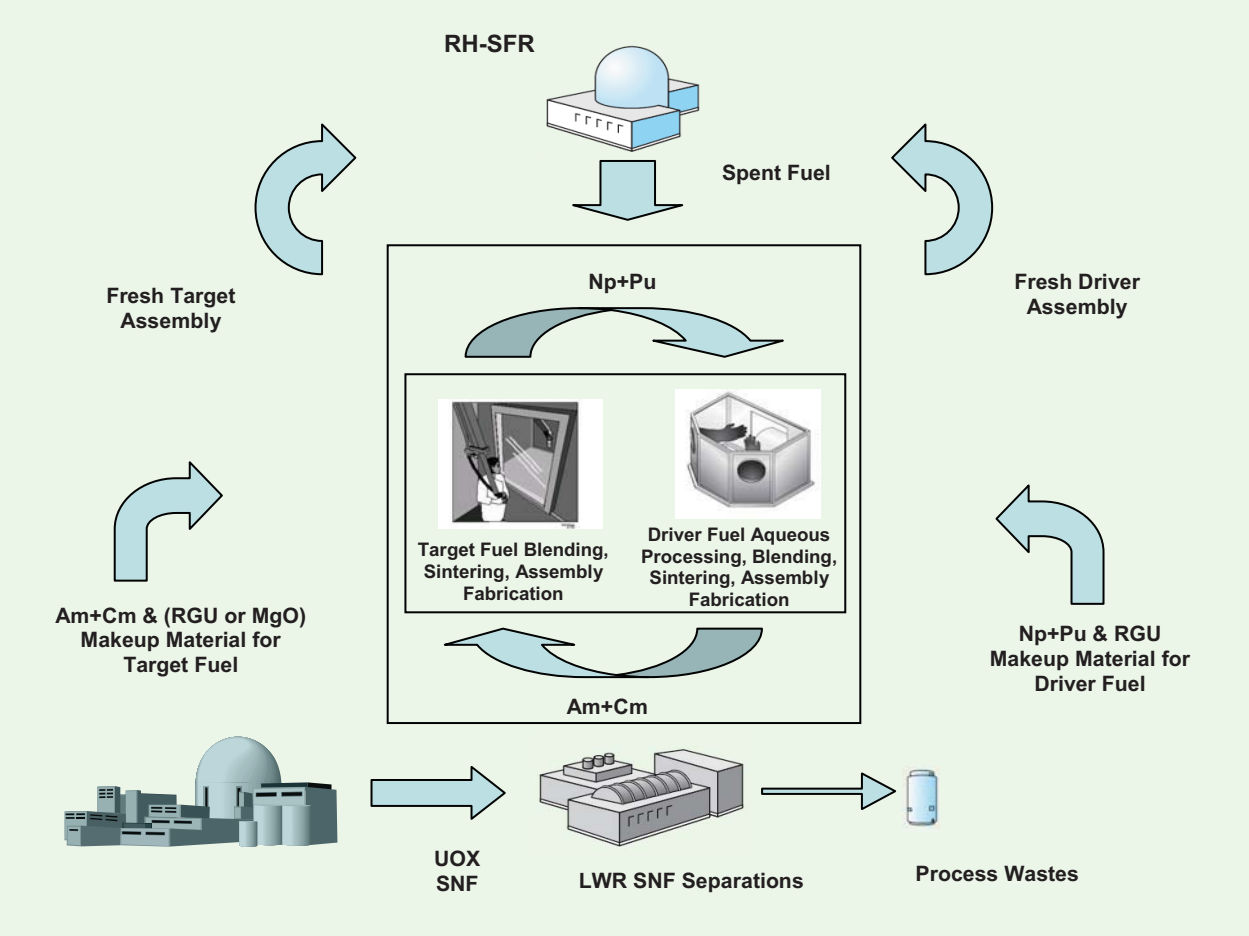

Figure 2: Heterogeneous recycling scheme

3.3 External Feed from Light Water Reactor Spent Fuel

The external feed of TRU to the fast reactor is assumed to come from once-burned LWR SNF which had achieved a burnup of 50 MWd/kg and was cooled for five years before reprocessing. Table 2 shows the isotopic vectors for both the Np+Pu external feed to the drivers and the MA external feed to the targets. Both mass fraction columns in Table 2 sum to unity. However, the ratio of external feed rate to targets (MA) and external feed rate to drivers (Np+Pu) is kept constant and equal to the ratio found in LWR spent fuel having the decay times mentioned above (the value used in this work was 0.06257). Note that the Np+Pu external feed, shown in Table 2, is not completely free of Am-241. This Am-241 comes from the 2-year post-separation decay time allotted for fabrication and transportation to the reactor.

Table 2. Composition (in mass fraction) of external feed from LWR spent fuel.

Nuclide	Np+Pu Feed to Drivers	MA Feed to Targets
U-234	4.169E-04	2.414E-07
U-235	2.772E-05	2.901E-09
U-236	4.989E-05	8.298E-07
U-238	2.716E-07	5.701E-12
Np-237	5.875E-02	1.755E-03
Pu-238	2.661E-02	2.553E-05
Pu-239	4.901E-01	1.023E-04
Pu-240	2.401E-01	7.888E-03
Pu-241	9.942E-02	9.906E-07
Pu-242	7.442E-02	3.120E-06
Am-241	1.006E-02	5.557E-01
$Am-242^{m}$	0.000E+00	1.694E-03
Am-243	0.000E+00	3.238E-01
Cm-242	0.000E+00	4.996E-06
Cm-243	0.000E+00	8.719E-04
Cm-244	0.000E+00	1.008E-01
Cm-245	0.000E+00	6.475E-03
Cm-246	0.000E+00	8.367E-04
Cm-247	0.000E+00	1.319E-05
Cm-248	0.000E+00	9.586E-07
Cf-249	0.000E+00	1.327E-08
Cf-250	0.000E+00	3.911E-09
Cf-251	0.000E+00	2.281E-09
Cf-252	0.000E+00	2.497E-10

4. Analysis Results

4.1 Transmutation Performance

Table 3 shows the results of three cases modeled for the comparison of MgO and UO_2 matrix options. The first two columns (A and B) represent the replacement of MgO with UO_2 matrix while leaving the geometry of the drivers and targets unchanged. In examining these two cases, one observes that while the MgO matrix case has a CR of 0.73, the UO_2 matrix case has the significantly higher value of 0.87. The plutonium bred from U-238 creates a significant source of TRU in the UO_2 target case. This plutonium that is bred in the targets is reloaded in the driver fuel as a priority before external feed is added to meet the transuranic enrichment requirement. This reduces by roughly a factor of two the external feed of LWR Np+Pu required in the drivers to achieve the desired cycle length in the UO_2 matrix case. Because the ratio of external feed of MA to Np+Pu is fixed to the isotopics of LWR spent fuel, the external feed rate of MA into the targets is reduced by the same factor.

Table 3. Performance of MgO and UO_2 target cases.

Matrix Material		**MgO**	**UO_2**	
Case Label		**A**	**B**	**C**
Driver Fuel Volume Fraction		0.40	0.40	0.35
Target Fuel Volume Fraction		0.40	0.40	0.35
TRU CR		0.73	0.87	0.73
Cycle Length (d)		344	353	340
# of Cycles Targets Remain in Core		10	10	10
TRU Enrichment (volume % TRU O_2)	Inner Core	21.1	19.9	24.5
	Middle Core	26.4	24.9	30.6
	Outer Core	31.7	29.9	36.8
	Targets	9.7	8.8	14.5
Peak Flux ($x10^{15}cm^{-2}s^{-1}$)	Outer Drivers	3.08	3.03	3.11
	Targets	2.19	2.09	2.18
Peak Fast Flux ($x10^{15}cm^{-2}s^{-1}$)	Outer Drivers	1.89	1.85	1.92
	Targets	1.21	1.23	1.30
Peak Fast Fluence ($x10^{23}cm^{-2}$)	Outer Drivers	3.95	3.95	3.94
	Targets	3.60	3.74	3.80
DPA (limit = 200)	Outer Drivers	198	200	199
	Targets	150	167	171
External TRU Feed Rates (kg/EFPY)	TRU	87.1	39.5	89.5
	MA	5.16	2.35	5.33
Target Decay heat (kW/bundle)	BOEC	0.71	0.56	0.84
	EOEC	2.3	3.1	3.7
	1 year cooled	0.80	0.74	1.0
	5 year cooled	0.50	0.42	0.63

In order to compare the two matrix materials on the basis of equal TRU destruction rate, a second UO_2 matrix case was generated with a lower fuel volume fraction in order to bring the CR down to 0.73, equal to the MgO case. The fuel volume fraction required in this reduced CR case was approximately 35%. This volume fraction was used in both the drivers and the targets. The results from this case are in column C. Unless otherwise specified, the UO_2 case being compared to the MgO case is the one having CR = 0.73 (case C) for the remainder of this report.

The cycle lengths required to reach the 200 dpa limit in the outer drivers (the limiting region in cases A and C) are about the same at 340 and 344 days for the UO_2 and MgO cases, respectively. The TRU and MA external feed rates are approximately the same for the two cases since their CR values have been forced equal and the reactor power is constant between the two cases. The target enrichment in the UO_2 case is 14.5% versus 9.7% in the MgO case. One reason for the higher enrichment in the UO_2 matrix case is that the fuel volume fraction in the targets is reduced in the UO_2 case, which means that the same amount of MA material would occupy a greater fraction of the space in the target, leading to a higher enrichment value. This, however, does not explain completely the increase in enrichment from the MgO to UO_2 matrix options of equal CR. There is, in fact, a 30% larger inventory of MA in the UO_2 targets than in the MgO targets.

Table 4 shows the charge and discharge rates of HM in kg/EFPY in target and driver assemblies for UO_2 and MgO cases having CR = 0.73.[a] From this table, one sees that the amount of uranium loaded into the drivers varies significantly between the two cases, yet the amount of Np+Pu loaded into the driver fuel is roughly the same between the two cases. This is because the amount of Np+Pu loaded in the driver fuel is the main determinant in the reactivity-limited cycle length, which is about the same in both cases since it is determined by the dpa in the outer fuel zone. The difference in uranium present in the drivers is a result of the larger fuel volume fraction in the MgO case than in the UO_2 case. In the driver fuel, the net production of minor actinides is approximately the same in each case. This is because although there is more uranium in the drivers in the MgO case, most of the MA production comes from Np+Pu, which is approximately equal in the two cases.

Table 4. HM charge and discharge rates (in kg/EFPY) in target and driver assemblies for UO_2 and MgO cases having CR = 0.73.

		MgO Matrix (CR=0.73)			UO_2 Matrix (CR=0.73)		
		Charge	Discharge	Net Change	Charge	Discharge	Net Change
Drivers	U	1967	1678	-289	1642	1364	-278
	Np+Pu	648	558	-90	663	528	-135
	Am+Cm+Bk+Cf	0.82	16.1	15.3	0.85	15.9	15.1
Targets	U	0.0	0.20	0.20	410	367	-43
	Np+Pu	0.05	10.11	10.06	0.05	40.17	40.12
	Am+Cm+Bk+Cf	52.8	30.1	-22.7 E_{MA} = 43%	69.5	46.6	-22.9 E_{MA} = 33%

The 'Targets' rows in Table 4 show that although the net change in MA is approximately equal between the two cases, the charge and discharge rates are higher in the UO_2 matrix case than in the MgO matrix case, showing that the mass inventory of MAs in the UO_2 targets is 30% larger than in the MgO target case. Figure 3 shows a schematic representation of the MA mass flow rates into and out of the

[a] Tables can be found in the Appendix giving the data in Table 4 expanded to include each nuclide separately.

targets. The MA flow into the targets comes from external MA feed and MAs recycled from the drivers and the sum of these two inputs is equal to the MA destruction minus the MA production within the targets. Because the whole-core CR is the same between the two cases, the external feed of MA from LWR spent fuel is equal between the MgO and UO_2 target cases. Also, the feed rate of MA recycled from drivers is about the same as seen from the driver MA discharge rates in Table 4. Within the targets, there are MA production terms (through successive neutron captures starting from uranium) and MA destruction terms which sum to approximately the same value in each case. The destruction rate minus the production rate must therefore be constant between the two cases. In the MgO case, the MA production term is zero because the HM loading is all MAs. In the UO_2 case, however, there is U-238 present, which during the 10 cycles of irradiation, serves as a MA source. Therefore, the destruction rate of MAs in the targets must be higher in the UO_2 case to compensate for the production term in order to achieve the same net destruction rate. This is achieved by having a higher MA number density at BOEC. This higher inventory of MAs in the UO_2 targets is reflected in the target MA charge and discharge data shown in Table 4, as well as in the higher enrichment in the UO_2 matrix case.

The MA destruction efficiency (E_{MA}) of the targets is defined as the absolute value of MA mass in a target assembly at discharge minus the amount charged in that fresh assembly, divided by the amount in the fresh assembly. It is a measure of how completely the MAs are destroyed during the in-core life of a target assembly. These values are given in the bottom row in Table 4 along with the net change numbers. Although the two cases shown have the same net destruction rates of MA, the higher inventory of MA charged in the UO_2 matrix case gives it a lower E_{MA} value of 33% versus the 43% value for the MgO cases.

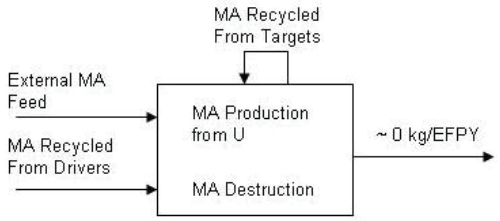

Figure 3. Schematic of MA mass balance in target assemblies.

The major disadvantages of the higher MA enrichment required in the UO_2 matrix case is a significantly higher decay heat per target assembly than in the MgO case, as is shown in Table 3, complicating the handling of the target fuel assemblies.

4.2 Helium and Fission Gas Production

Table 5 shows the atoms of helium, krypton and xenon produced in the target assemblies during 10 cycles of irradiation (units of total atoms $\times 10^{-24}$). These results represent the atoms produced without taking into account what fraction is released from the fuel. The values are given for each responsible nuclide for the three gases and then totals for each gas are displayed at the bottom of each column. The xenon and krypton totals are significantly higher for the UO_2 targets than for the MgO targets. This is a result of the greater number of fissions which occur in the UO_2 targets, a result of higher enrichment. The number of helium atoms produced in the UO_2 targets exceeds that of the MgO case, but not by a factor similar to the difference in MA charged into the different target types. As seen in

Table 5, the two main producers of helium are Cm-242 and Cm-244. Pu-238 and Am-241 are the next two largest helium producers in the target assemblies. The contributors to the helium produced are shown graphically in Figure 4. These four nuclides contribute the vast majority of helium production in the targets due to their high alpha activity. The total helium produced, therefore, is quite sensitive to differences in the inventory of these four nuclides, particularly these two curium nuclides. Because the production of Cm-242, due to its short half-life, is approximately in secular equilibrium with the transmutation of Am-241, its helium generation rate is also strongly coupled with the destruction of Am-241.

Figure 5 shows the mass of Cm-242 in the target assemblies versus irradiation time in Effective Full Power Year (EFPY) for the MgO and UO_2 target matrix cases having CR=0.73. Although the UO_2 targets have a 30% larger total MA loading, the time-integrated amount of Cm-242 present in the UO_2 targets during their life is slightly lower than in the MgO targets. Although the mass of Cm-242 present in either case represents at most 0.5% of the MA mass present in the fresh target, this small difference has a large effect on helium production due to the very high alpha activity of this nuclide ($T_{1/2,\alpha}$ =162.8 days).

Table 6 shows gas plenum partial pressures in the target assemblies at the end of the 10-cycle irradiation for MgO and UO_2 matrix cases having CR = 0.73 assuming 85% of the gas atoms produced are released from the fuel. The effect of the different production rates of helium, krypton and xenon resulted in a significantly higher plenum pressure in the targets having UO_2 matrix than those having MgO matrix. This is primarily due to the larger amount of fissions occurring in the targets having UO_2 matrix.

Table 5. Atoms ($x10^{-24}$) of helium, krypton and xenon produced in the target assemblies during 10 cycles of irradiation.

	MgO Targets CR = 0.73 (3440 days)			**UO_2 Targets CR = 0.73** (3440 days)		
Nuclide	**He**	**Kr**	**Xe**	**He**	**Kr**	**Xe**
U-234	1.50E-06	6.64E-04	9.54E-04	2.85E-06	1.30E-03	1.87E-03
U-235	4.59E-11	6.44E-04	9.25E-04	1.56E-08	1.36E-01	1.95E-01
U-236	2.18E-10	3.11E-06	4.46E-06	5.40E-07	6.93E-03	9.96E-03
U-238	5.86E-15	3.82E-09	8.48E-09	4.34E-07	2.85E-01	6.31E-01
Np-237	1.81E-07	4.59E-04	1.02E-03	8.83E-07	2.45E-03	5.44E-03
Np-238	0.00E+00	0.00E+00	0.00E+00	0.00E+00	0.00E+00	0.00E+00
Pu-236	2.22E-07	7.95E-09	1.14E-08	1.25E-06	3.57E-08	5.12E-08
Pu-238	1.74E-01	8.81E-02	1.95E-01	1.70E-01	7.35E-02	1.63E-01
Pu-239	8.09E-05	1.56E-02	5.45E-02	3.17E-03	4.22E-01	1.47E+00
Pu-240	1.29E-03	7.49E-03	2.62E-02	2.24E-03	1.34E-02	4.69E-02
Pu-241	0.00E+00	6.75E-03	3.17E-02	0.00E+00	3.88E-03	1.82E-02
Pu-242	1.16E-05	2.01E-03	9.43E-03	1.07E-05	1.92E-03	9.01E-03
Am-241	1.36E-01	2.92E-02	1.37E-01	2.19E-01	4.69E-02	2.20E-01
$Am\text{-}242^{m}$	1.76E-04	7.55E-02	3.55E-01	2.79E-04	7.22E-02	3.39E-01
Am-243	6.71E-03	1.85E-02	8.69E-02	1.14E-02	3.25E-02	1.52E-01
Cm-242	5.61E+00	6.84E-04	3.21E-03	5.32E+00	6.75E-04	3.17E-03
Cm-243	1.68E-02	4.49E-03	2.11E-02	1.13E-02	1.82E-03	8.53E-03
Cm-244	2.86E+00	3.93E-02	1.85E-01	3.31E+00	4.53E-02	2.13E-01
Cm-245	2.25E-03	1.49E-01	6.99E-01	2.23E-03	1.05E-01	4.92E-01
Cm-246	3.01E-03	6.39E-03	3.00E-02	2.93E-03	6.34E-03	2.97E-02
Cm-247	1.76E-07	1.17E-02	5.49E-02	1.01E-07	6.12E-03	2.87E-02
Cm-248	4.62E-06	8.78E-04	4.12E-03	2.83E-06	5.23E-04	2.45E-03
Bk-249	0.00E+00	9.89E-06	4.64E-05	0.00E+00	2.82E-06	1.32E-05
Cf-249	5.48E-04	1.61E-03	7.55E-03	2.36E-04	4.59E-04	2.16E-03
Cf-250	5.37E-03	1.29E-04	6.06E-04	9.98E-04	2.66E-05	1.25E-04
Cf-251	2.40E-05	1.38E-04	6.50E-04	2.58E-06	1.13E-05	5.31E-05
Cf-252	4.78E-04	2.94E-06	1.38E-05	3.06E-05	1.12E-07	5.25E-07
Total	**8.82E+00**	**4.59E-01**	**1.90E+00**	**9.06E+00**	**1.26E+00**	**4.04E+00**

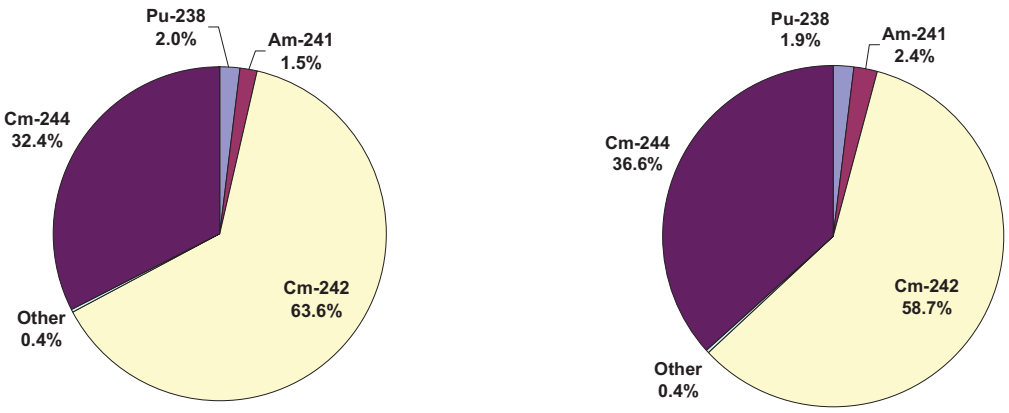

Figure 4. Contributions to helium generation from four major nuclides in target assemblies in cases having CR = 0.73 for the MgO case (left) and UO_2 case (right).

Table 6. Target pin plenum partial pressures (in atm) at end of 10-cycle irradiation for cases with MgO and UO_2 target matrix having CR = 0.73.

Matrix Material	He	Kr	Xe	Total
MgO (3440 days)	29.5	1.54	6.37	37.4
UO_2 (3400 days)	34.9	4.85	15.5	55.3

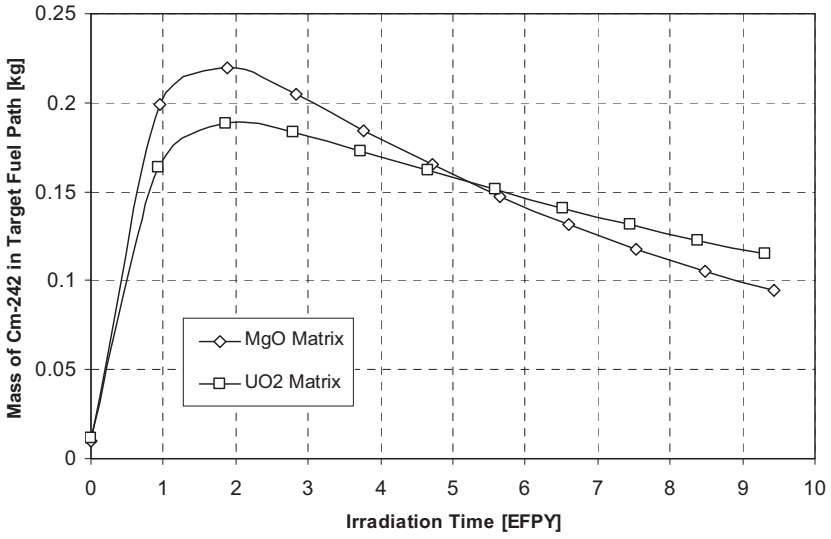

Figure 5. Mass of Cm-242 in target assemblies versus irradiation time in EFPY for cases having CR=0.73.

5. Summary and Conclusions

The primary focus of this work was the comparison of MgO and UO_2 target matrix materials based on oxide cores having the same CR, thus matching the overall MA and TRU destruction rates between the two cases of interest. The same number of target assemblies was used in each case (48) and approximately the same cycle length was used based on the 200 dpa limit in the outer driver zone. In order to maintain a CR of 0.73, the MgO matrix case had a fuel volume fraction of 40%, while the UO_2 volume fraction was reduced to 35% in order to compensate for the plutonium breeding occurring in the UO_2 used as matrix material in that case. The fuel volume fraction for the targets was kept the same as that used for the driver fuel in each core design.

The UO_2 matrix-based targets required a 30% higher MA loading in order to achieve the same *net* MA destruction rate as the targets with an inert MgO matrix. The larger MA loading for the UO_2 case is due to the fact that the UO_2 target had a smaller transmutation efficiency than the MgO case. The transmutation efficiencies were 33% and 43%, for the UO_2 and MgO cases, respectively. Because of the introduction of an internal MA source term in the UO_2 matrix through successive neutron captures in heavy nuclides starting with U-238, the overall charge rate of MAs loaded in the targets has to be increased in order to arrive at the same *net* destruction rate as the MgO case. Given the assumptions in this analysis, this is done only through higher charge enrichment in the targets, hence the higher MA inventory in the UO_2 matrix case.

In this analysis, the number of targets and their residence time is approximately equal. Therefore, roughly the same number of target assemblies are handled (i.e.: loaded and discharged from the core) per EFPY, but with significantly higher decay heat in the UO_2 assemblies. One caveat of the comparison made in this work was that the target assemblies were not perfectly optimized to reach the 200 dpa limit. The possibility of leaving these targets in the core longer could be explored in order to increase the MA destruction efficiency. The tradeoff is that with the longer residence time, there are fewer assemblies per EFPY to handle in reprocessing. However, to achieve the same net MA destruction rate, they would have to be charged with a higher MA enrichment and thus each individual assembly might be more complicated to handle.

The higher MA inventory present in the targets having UO_2 matrix leads to higher pin pressures at the end of target assembly life. In this analysis, the pressures in the UO_2 matrix targets are made even higher due to the lower fuel volume fraction. However, even based on equal volume of fuel, the UO_2 targets would still have greater gas pressures. The reasons for this are twofold. First, these assemblies have a greater number of fissions taking place. Therefore, the fission gasses Xe and Kr will have a greater buildup in the targets having UO_2 matrix. Secondly, because there is a larger MA inventory, alpha decay of MAs creates more helium in the targets having UO_2 matrix.

If fewer target assemblies are used to burn external TRU at the same rate as the 48 target case investigated here, the resulting enrichments in the targets would be higher. Thus, the resulting amount of UO_2 matrix would be smaller in the UO_2 case. Therefore, the differences in performance between the MgO case and UO_2 cases would become less extreme as the number of target assemblies used is decreased. Furthermore, because the differences in performance between these two matrix options are driven largely by MA production from the UO_2 matrix material, shorter target residence times would likely lead to less pronounced differences between the two matrix options as well, since during a short irradiation time, the amount of MAs produced would be decreased.

6. References

1. Gelles, D., (1994), Microstructural Development in Reduced Activation Ferritic Alloys Irradiated to 200 dpa at 420 oC, Journal of Nuclear Materials, 212, 714-719

2. Hoffman, E., Yang, W., Hill, R. (2006) Preliminary Core Design Studies for the Advanced Burner Reactor Over a Wide Range of Conversion Ratios, Argonne National Laboratory, ANL-AFCI-177

3. Bays S., Pope M., Forget B., Ferrer R., (2008), Neutronic Assessment of Transmutation Target Compositions in Heterogeneous Sodium Fast Reactor Geometries, INL/EXT-07-13643

4. Henryson, H., Toppel, B., Stenberg, C., (1976), MC2-2: A Code to Calculate Fast Neutron Spectra and Multigroup Cross Sections, ANL-8144

5. Derstine, K., (1984), DIF3D: A Code to Solve One-, Two-, and Three-Dimensional Finite-Difference Diffusion Theory Problems, ANL-82-64

6. Toppel, B. (1983), A User's Guide to the REBUS-3 Fuel Cycle Analysis Capability, Argonne National Laboratory, ANL-83-2

7. Walter, A., Reynolds, A., (1981), "Fast Breeder Reactors", Pergamon Press Inc., Maxwell House, Fairview Park, Elmsford, New York, United States

Appendix A

Target HM charge and discharge rates (in kg/EFPY) for MgO matrix option with CR = 0.73.

Note: The isotopes less than Am-241 in the "Charge" column are produced by the two year decay period between SNF reprocessing and being loaded into the core.

Nuclide	Charge	Discharge	Net change	Charge	Discharge	Net change
U-234	1.25E-06	1.79E-01	1.79E-01	0.00	0.20	0.20
U-235	0.00E+00	2.14E-02	2.14E-02			
U-236	4.27E-06	3.49E-03	3.49E-03			
U-238	0.00E+00	1.31E-05	1.31E-05			
Np-237	9.05E-03	9.56E-02	8.66E-02	0.05	10.11	10.06
Np-238	0.00E+00	0.00E+00	0.00E+00			
Pu-236	0.00E+00	2.76E-07	2.76E-07			
Pu-238	1.32E-04	4.42E+00	4.42E+00			
Pu-239	5.27E-04	8.90E-01	8.90E-01			
Pu-240	4.07E-02	2.95E+00	2.91E+00			
Pu-241	5.08E-06	3.92E-01	3.92E-01			
Pu-242	1.61E-05	1.35E+00	1.35E+00			
Am-241	1.89E+01	6.35E+00	-1.25E+01	52.80	30.12	-22.68 (E_{MA} = 43%)
Am-242	1.10E+00	7.62E-01	-3.40E-01			
Am-243	1.45E+01	6.26E+00	-8.26E+00			
Cm-242	3.11E-02	3.01E-01	2.70E-01			
Cm-243	9.64E-02	7.92E-02	-1.72E-02			
Cm-244	1.05E+01	9.00E+00	-1.54E+00			
Cm-245	3.85E+00	3.61E+00	-2.36E-01			
Cm-246	2.84E+00	2.82E+00	-1.45E-02			
Cm-247	5.48E-01	5.48E-01	-2.55E-04			
Cm-248	3.22E-01	3.22E-01	-1.27E-04			
Bk-249	1.66E-03	8.08E-03	6.42E-03			
Cf-249	4.44E-02	3.82E-02	-6.25E-03			
Cf-250	1.35E-02	1.50E-02	1.51E-03			
Cf-251	4.42E-03	4.43E-03	7.32E-06			
Cf-252	1.78E-04	2.96E-04	1.18E-04			

Driver HM charge and discharge rates (in kg/EFPY) for MgO matrix option with CR = 0.73.

Nuclide	Charge	Discharge	Net change	Charge	Discharge	Net change
U-234	4.01E-01	9.67E-01	5.66E-01	1967.02	1677.61	-289.41
U-235	1.49E+01	5.12E+00	-9.77E+00			
U-236	1.21E+01	1.09E+01	-1.12E+00			
U-238	1.94E+03	1.66E+03	-2.79E+02			
Np-237	1.33E+01	8.37E+00	-4.96E+00	647.74	558.44	-89.30
Np-238	0.00E+00	0.00E+00	0.00E+00			
Pu-236	5.48E-05	8.87E-05	3.40E-05			
Pu-238	2.27E+01	1.58E+01	-6.89E+00			
Pu-239	3.00E+02	2.59E+02	-4.11E+01			
Pu-240	2.22E+02	1.98E+02	-2.34E+01			
Pu-241	3.80E+01	3.24E+01	-5.59E+00			
Pu-242	5.20E+01	4.46E+01	-7.45E+00			
Am-241	8.25E-01	6.78E+00	5.95E+00	0.82	16.09	15.27
Am-242	0.00E+00	3.41E-01	3.41E-01			
Am-243	0.00E+00	6.59E+00	6.59E+00			
Cm-242	0.00E+00	3.36E-01	3.36E-01			
Cm-243	0.00E+00	1.73E-02	1.73E-02			
Cm-244	0.00E+00	1.81E+00	1.81E+00			
Cm-245	0.00E+00	2.03E-01	2.03E-01			
Cm-246	0.00E+00	9.53E-03	9.53E-03			
Cm-247	0.00E+00	2.17E-04	2.17E-04			
Cm-248	0.00E+00	6.93E-06	6.93E-06			
Bk-249	0.00E+00	8.79E-08	8.79E-08			
Cf-249	0.00E+00	4.65E-08	4.65E-08			
Cf-250	0.00E+00	6.58E-09	6.58E-09			
Cf-251	0.00E+00	1.64E-10	1.64E-10			
Cf-252	0.00E+00	2.90E-12	2.90E-12			

Target HM charge and discharge rates (in kg/EFPY) for UO_2 matrix option with CR = 0.73.

Nuclide	Charge	Discharge	Net change	Charge	Discharge	Net change
U-234	7.65E-02	2.50E-01	1.73E-01	409.91	366.63	-43.28
U-235	3.10E+00	1.41E+00	-1.69E+00			
U-236	2.51E+00	2.39E+00	-1.25E-01			
U-238	4.04E+02	3.63E+02	-4.16E+01			
Np-237	9.36E-03	6.39E-01	6.30E-01	0.05	40.17	40.12
Np-238	0.00E+00	0.00E+00	0.00E+00			
Pu-236	0.00E+00	2.01E-06	2.01E-06			
Pu-238	1.36E-04	5.08E+00	5.08E+00			
Pu-239	5.45E-04	2.64E+01	2.64E+01			
Pu-240	4.21E-02	6.20E+00	6.16E+00			
Pu-241	5.26E-06	3.98E-01	3.98E-01			
Pu-242	1.66E-05	1.40E+00	1.40E+00			
Am-241	2.61E+01	1.33E+01	-1.27E+01	69.46	46.59	-22.87 (E_{MA} = 33%)
Am-242	1.79E+00	1.46E+00	-3.34E-01			
Am-243	2.15E+01	1.31E+01	-8.43E+00			
Cm-242	3.60E-02	3.70E-01	3.34E-01			
Cm-243	7.45E-02	5.61E-02	-1.84E-02			
Cm-244	1.26E+01	1.12E+01	-1.42E+00			
Cm-245	3.95E+00	3.71E+00	-2.41E-01			
Cm-246	2.84E+00	2.82E+00	-1.37E-02			
Cm-247	3.23E-01	3.22E-01	-3.22E-04			
Cm-248	2.02E-01	2.02E-01	-2.25E-05			
Bk-249	4.79E-04	2.33E-03	1.85E-03			
Cf-249	1.88E-02	1.70E-02	-1.78E-03			
Cf-250	2.56E-03	2.85E-03	2.86E-04			
Cf-251	4.87E-04	4.87E-04	7.73E-07			
Cf-252	1.17E-05	1.94E-05	7.72E-06			

Driver HM charge and discharge rates (in kg/EFPY) for UO_2 matrix option with CR = 0.73.

Nuclide	Charge	Discharge	Net change	Charge	Discharge	Net change
U-234	3.42E-01	9.27E-01	5.86E-01	1641.57	1364.09	-277.48
U-235	1.24E+01	4.18E+00	-8.24E+00			
U-236	1.01E+01	8.93E+00	-1.15E+00			
U-238	1.62E+03	1.35E+03	-2.69E+02			
Np-237	1.39E+01	8.05E+00	-5.86E+00	663.38	528.25	-135.13
Np-238	0.00E+00	0.00E+00	0.00E+00			
Pu-236	5.56E-05	8.61E-05	3.06E-05			
Pu-238	2.40E+01	1.59E+01	-8.06E+00			
Pu-239	3.07E+02	2.33E+02	-7.36E+01			
Pu-240	2.27E+02	1.95E+02	-3.22E+01			
Pu-241	3.87E+01	3.21E+01	-6.58E+00			
Pu-242	5.33E+01	4.45E+01	-8.80E+00			
Am-241	8.47E-01	6.68E+00	5.84E+00	0.85	15.92	15.07
Am-242	0.00E+00	3.33E-01	3.33E-01			
Am-243	0.00E+00	6.54E+00	6.54E+00			
Cm-242	0.00E+00	3.32E-01	3.32E-01			
Cm-243	0.00E+00	1.68E-02	1.68E-02			
Cm-244	0.00E+00	1.80E+00	1.80E+00			
Cm-245	0.00E+00	2.02E-01	2.02E-01			
Cm-246	0.00E+00	9.53E-03	9.53E-03			
Cm-247	0.00E+00	2.21E-04	2.21E-04			
Cm-248	0.00E+00	7.11E-06	7.11E-06			
Bk-249	0.00E+00	9.23E-08	9.23E-08			
Cf-249	0.00E+00	4.79E-08	4.79E-08			
Cf-250	0.00E+00	7.22E-09	7.22E-09			
Cf-251	0.00E+00	1.86E-10	1.86E-10			
Cf-252	0.00E+00	3.35E-12	3.35E-12			